

Twist and Turn: Weak Lensing Image Distortions to Second Order

David J. Bacon^{1*} & Björn Malte Schäfer²

¹ *Institute of Cosmology and Gravitation, University of Portsmouth, Mercantile House, Hampshire Terrace, Portsmouth, PO1 2EG, United Kingdom*

² *Institut d'Astrophysique Spatiale, Université de Paris XI, Bâtiment 120-121, Centre Universitaire d'Orsay, 91400 Orsay CEDEX, France*

1 November 2018

ABSTRACT

We account for all the image distortions relevant to weak gravitational lensing to second order. Besides the familiar shear, convergence, rotation and flexions, we find two new image distortions, the twist and the turn. Like rotation, these are not activated gravitationally to first order, but will be activated by systematic effects. We examine the rotational properties of twist and turn, and their effect on images in real and shapelet space. We construct estimators for the new distortions, taking into account the centroid shift which they generate. We then use these estimators to make first measurements of twist and turn using the STAGES HST survey; we find that the mean twist and turn are consistent with zero. We measure twist and turn correlation functions for the survey, again finding little evidence of systematic effects.

Key words: cosmology: observations – gravitational lensing.

1 INTRODUCTION

Weak gravitational flexion is a relatively new addition to the panoply of gravitational lensing effects, but has considerable potential for measuring substructure in the density distribution of matter in the Universe (see e.g. Goldberg & Natarajan 2002; Goldberg & Bacon 2005; Irwin & Shmakova 2005; Bacon et al. 2006; Okura et al. 2008; Schneider & Er 2008).

Flexion is proportional to third angular derivatives of the projected gravitational potential along the line of sight. As such, it is at the next order of differentiation compared to shear and convergence, which are the more studied weak lensing measures (see Bartelmann & Schneider 2001, for an extensive review). Since, as we shall see, there are two independent combinations of third derivatives, there are two different flexion effects: the 1-flexion, which is a vector distortion leading to objects being skewed; and the 3-flexion, which is a spin three distortion changing circular objects into trefoils.

Up until now, these have been the only known image distortions at this order. However, in this paper we will show that there are two further neglected image distortions at the flexion level, which we call twist and turn for reasons which will become obvious. These are not activated by gravity under the most straightforward approximations; but they will be activated by systematic effects. The latter are of great concern to weak lensing, so finding further signatures of systematics is potentially very valuable to upcoming lensing surveys.

In this paper we show how twist and turn arise, and account for why they have not been noticed before. We show how they affect images in real and shapelet space, and give details of how they can be measured with fairly straightforward estimators. We then

measure twist and turn for the first time using the Space Telescope A901/902 Galaxy Evolution Survey (STAGES, Gray et al. 2007), a large mosaic observed with the Hubble Space Telescope (HST). We show that these measures are almost all currently consistent with zero for STAGES, for both their mean values and their correlation functions, incrementally adding confidence in the management of systematics for this survey.

The paper is organised as follows. In Section 2, we recount the theory of image distortions in weak lensing at the more studied first order. We note that there is already a non-gravitational mode at this order; image rotation. We write the distortions in terms of Pauli matrices, which will give us the necessary clues for how to treat higher order distortions later.

In Section 3, we extend the account to second order. We find that there are combinations of Pauli matrices orthogonal to those describing the conventional flexion degrees of freedom; these orthogonal combinations give twist and turn distortions. We are therefore able to write down for the first time the complete weak image distortion to second order.

Section 4 describes the behaviour of twist and turn. The rotational properties of the distortions are worked out, and we find that both distortions are vector quantities. We show the impact of twist and turn on simple images; we find that they do not affect the shape of circularly symmetric images, but only images with non-zero ellipticity. We show explicitly the nature of twist and turn in shapelet space, proving that they have no impact on circularly symmetric sources, and derive how they move power between shapelet coefficients.

In Section 5 we go about finding practical estimators for measuring twist and turn. We derive simple estimators in shapelet space. Noting that like flexion, twist and turn affect the centroids of objects, we correct the estimators by constructing slightly more complicated expressions which take this shift into account.

* E-mail: david.bacon@port.ac.uk

In Section 6 we use these estimators to make the first measurements of twist and turn, using the STAGES HST survey. We find that twist and turn have larger variances than flexion, and that their mean value is consistent with zero in the STAGES data. We measure correlation functions for the two distortions, again finding that they are mainly consistent with zero systematics in STAGES. We summarise our results and conclude in Section 7.

2 IMAGE DISTORTIONS TO FIRST ORDER

We begin by discussing image distortions in weak lensing to first order (for more details, see Bartelmann & Schneider 2001). We can describe the effect of lensing as a mapping between the surface brightness f_S of a galaxy at a position (β_1, β_2) in the source plane, and the surface brightness f_I at a position (θ_1, θ_2) in the image plane:

$$f_I(\theta_i) = f_S(\beta_i) = f_S(A_{ij}\theta_j) \quad (1)$$

where we have set the origin of θ_i and β_i to the centre of light in the respective planes. A is the Jacobian matrix which maps image positions to source positions,

$$A_{ij} = \frac{\partial \beta_i}{\partial \theta_j}. \quad (2)$$

For lensing with a single lens plane, and assuming the Born approximation, this is given by

$$A_{ij} = \delta_{ij} - \partial_i \partial_j \psi \quad (3)$$

where ψ is the lensing potential, i.e. the gravitational potential suitably projected into 2D. We can therefore write A as

$$A = \begin{pmatrix} 1 - \kappa & 0 \\ 0 & 1 - \kappa \end{pmatrix} + \begin{pmatrix} -\gamma_1 & -\gamma_2 \\ -\gamma_2 & \gamma_1 \end{pmatrix} \quad (4)$$

with the convergence κ given by

$$\kappa = \frac{1}{2}(\partial_1^2 + \partial_2^2)\psi \quad (5)$$

and the shear γ_i given by

$$\gamma_1 = \frac{1}{2}(\partial_1^2 - \partial_2^2)\psi, \quad \gamma_2 = \partial_1 \partial_2 \psi. \quad (6)$$

There is an alternative notation that is useful to us, introduced by Bacon et al. (2006). We define the complex derivative $\partial \equiv \partial_1 + i\partial_2$; in cylindrical coordinates this is given by

$$\partial = e^{i\phi} \left(\frac{\partial}{\partial \theta} + i \frac{\partial}{\partial \phi} \right) \quad (7)$$

with radial coordinate θ and azimuthal coordinate ϕ . We also define $\gamma \equiv \gamma_1 + i\gamma_2$, and then

$$\kappa = \frac{1}{2}\partial\partial^*\psi, \quad \gamma = \frac{1}{2}\partial\partial\psi. \quad (8)$$

Besides simplifying notation, this format elucidates the spins of the quantities; when ∂ is applied, the $e^{i\phi}$ term in equation (7) raises the spin by one. Similarly, the application of ∂^* lowers the spin by one. So since ψ is a scalar, so is κ , while γ is spin 2.

However, our study of A is not complete. We have specified three quantities in A , i.e. κ , γ_1 , and γ_2 . But A is a four element object, so there is a further degree of freedom which we have missed. We quickly realise that this is a **rotation** ρ , i.e.

$$A = \begin{pmatrix} 1 - \kappa & 0 \\ 0 & 1 - \kappa \end{pmatrix} + \begin{pmatrix} -\gamma_1 & -\gamma_2 \\ -\gamma_2 & \gamma_1 \end{pmatrix} + \begin{pmatrix} 0 & \rho \\ -\rho & 0 \end{pmatrix} \quad (9)$$

for small rotation angles ρ . Whereas κ and γ can be written as second derivatives of the lensing potential, this is not possible for ρ . It is not activated by gravity in our approximation (due to the interchangability of the second derivatives of the gravitational potential, $\partial_i \partial_j \psi = \partial_j \partial_i \psi$), but may be present in a real lensing survey as a systematic; in fact, it is the origin of the B-modes in lensing studies.

We will find it convenient to write A as a sum of Pauli matrices, as these provide an orthogonal basis for studying further degrees of freedom at the next order of weak lensing approximation. The Pauli matrices are given by (Arfken & Weber 2005)

$$\begin{aligned} I &= \begin{pmatrix} 1 & 0 \\ 0 & 1 \end{pmatrix} & \sigma_1 &= \begin{pmatrix} 0 & 1 \\ 1 & 0 \end{pmatrix} \\ \sigma_2 &= \begin{pmatrix} 0 & -i \\ i & 0 \end{pmatrix} & \sigma_3 &= \begin{pmatrix} 1 & 0 \\ 0 & -1 \end{pmatrix} \end{aligned} \quad (10)$$

so we can write A as

$$A = (1 - \kappa)I - \gamma_1\sigma_3 - \gamma_2\sigma_1 + \rho i\sigma_2. \quad (11)$$

We will need one further concept: in a weak lensing context, it is usual to assume that the shear and convergence are small and constant across an object. We can then write the surface brightness mapping as

$$f_I(\theta_i) = f_S(\delta_{ij}\theta_j + (A_{ij} - \delta_{ij})\theta_j) \simeq f_S(\theta_i) + (A_{ij} - \delta_{ij})\theta_j \partial_i f_S(\theta_i) \quad (12)$$

We will now modify this to show how flexion and the new distortions enter.

3 IMAGE DISTORTIONS TO SECOND ORDER

The further step taken by flexion studies is to note that in reality, shear will vary across an object. If we keep A as a constant across the object, we need a further term in a Taylor expansion in the surface brightness map, as given by Goldberg & Bacon (2005),

$$f_I(\theta_i) = f_S \left(A_{ij}\theta_j + \frac{1}{2}D_{ijk}\theta_j\theta_k \right). \quad (13)$$

This introduces the D tensor; if we suppose that its components are purely due to a variation of A across the image, we can write $D_{ijk} = \partial_k A_{ij}$. Then by differentiating equation (11) we find

$$\begin{aligned} D_{ij1} &= -\partial_1 \kappa I - \partial_1 \gamma_1 \sigma_3 - \partial_1 \gamma_2 \sigma_1 + \partial_1 \rho i\sigma_2, \\ D_{ij2} &= -\partial_2 \kappa I - \partial_2 \gamma_1 \sigma_3 - \partial_2 \gamma_2 \sigma_1 + \partial_2 \rho i\sigma_2. \end{aligned} \quad (14)$$

We can rewrite much of this in terms of flexion. We define the 1-flexion as $F \equiv F_1 + iF_2$, and the 3-flexion $G \equiv G_1 + iG_2$, where

$$F = \frac{1}{2}\partial\partial\partial^*\psi, \quad G = \frac{1}{2}\partial\partial\partial\psi. \quad (15)$$

F is manifestly spin 1 and G is spin 3. Comparing with equation (8) and disentangling the individual components we find

$$\begin{aligned} F_1 &= \partial_1 \kappa = \partial_1 \gamma_1 + \partial_2 \gamma_2, \\ F_2 &= \partial_2 \kappa = \partial_1 \gamma_2 - \partial_2 \gamma_1, \\ G_1 &= \partial_1 \gamma_1 - \partial_2 \gamma_2, \\ G_2 &= \partial_1 \gamma_2 + \partial_2 \gamma_1. \end{aligned} \quad (16)$$

Reorganising in terms of derivatives of shear, we can write

$$\begin{aligned}\partial_1 \gamma_1 &= \frac{1}{2}(F_1 + G_1), \\ \partial_2 \gamma_2 &= \frac{1}{2}(F_1 - G_1), \\ \partial_1 \gamma_2 &= \frac{1}{2}(F_2 + G_2), \\ \partial_2 \gamma_1 &= \frac{1}{2}(-F_2 + G_2).\end{aligned}\quad (17)$$

Hence we can write the D tensor in terms of the Pauli matrices as

$$\begin{aligned}D_{ij1} &= -F_1 I - \frac{1}{2}(F_1 + G_1)\sigma_3 - \frac{1}{2}(F_2 + G_2)\sigma_1 + \frac{1}{2}C_1 i\sigma_2 \\ D_{ij2} &= -F_2 I + \frac{1}{2}(F_2 - G_2)\sigma_3 - \frac{1}{2}(F_1 - G_1)\sigma_1 + \frac{1}{2}C_2 i\sigma_2\end{aligned}\quad (18)$$

where we have defined the **turn**,

$$C_i = 2\partial_i \rho \quad (19)$$

which in the complex notation we can write as $C = 2\partial\rho$, with $C \equiv C_1 + iC_2$. This is a new distortion mode, which simply describes how the amount of image rotation in the Jacobian varies across the object. Like the rotation, it is not expected to be activated by gravity at our level of approximation.

Separating into individual distortion components, we have

$$\begin{aligned}[-2D_{ij1}, -2D_{ij2}] &= F_1[2I + \sigma_3, \sigma_1] + F_2[\sigma_1, 2I - \sigma_3] \\ &\quad + G_1[\sigma_3, -\sigma_1] + G_2[\sigma_1, \sigma_3] \\ &\quad + C_1[-i\sigma_2, 0] + C_2[0, -i\sigma_2].\end{aligned}\quad (20)$$

F , G and C provide six parameters for D . However, D has eight components, so in general it possesses eight degrees of freedom. So what do the remaining two parameters represent? We note that whereas C premultiplies σ_2 , F and G premultiply mixtures of I , σ_1 and σ_3 . We are therefore seeking a further mixture of these latter quantities. We can find this by writing the six known objects as 1-D lists of elements, treating these as vectors and seeking two further vectors which are orthogonal to these six and each other. Gaussian elimination leads to the components

$$\begin{aligned}[-2D_{ij1}, -2D_{ij2}] &= \dots + T_1[-I + \sigma_1 + \sigma_3, -I + \sigma_1 - \sigma_3] \\ &\quad + T_2[-I - \sigma_1 + \sigma_3, I + \sigma_1 + \sigma_3].\end{aligned}\quad (21)$$

where we have introduced the **twist**, T , which is another non-gravitational mode. Unlike C , we cannot write T as a derivative of any previous mode; it arises only at second order.

So at last, we have a complete list of distortions to second order. Explicitly, the full image distortion to this order is described by the A matrix,

$$A = \begin{pmatrix} 1 - \kappa & 0 \\ 0 & 1 - \kappa \end{pmatrix} + \begin{pmatrix} -\gamma_1 & -\gamma_2 \\ -\gamma_2 & \gamma_1 \end{pmatrix} + \begin{pmatrix} 0 & \rho \\ -\rho & 0 \end{pmatrix} \quad (22)$$

and the D tensor,

$$\begin{aligned}-2D_{ij1} &= \begin{pmatrix} 3F_1 & F_2 \\ F_2 & F_1 \end{pmatrix} + \begin{pmatrix} G_1 & G_2 \\ G_2 & -G_1 \end{pmatrix} \\ &\quad + \begin{pmatrix} 0 & -C_1 \\ C_1 & 0 \end{pmatrix} + \begin{pmatrix} 0 & T_1 - T_2 \\ T_1 - T_2 & -2T_1 - 2T_2 \end{pmatrix} \\ -2D_{ij2} &= \begin{pmatrix} F_2 & F_1 \\ F_1 & 3F_2 \end{pmatrix} + \begin{pmatrix} G_2 & -G_1 \\ -G_1 & -G_2 \end{pmatrix} \\ &\quad + \begin{pmatrix} 0 & -C_2 \\ C_2 & 0 \end{pmatrix} + \begin{pmatrix} -2T_1 + 2T_2 & T_1 + T_2 \\ T_1 + T_2 & 0 \end{pmatrix}\end{aligned}\quad (23)$$

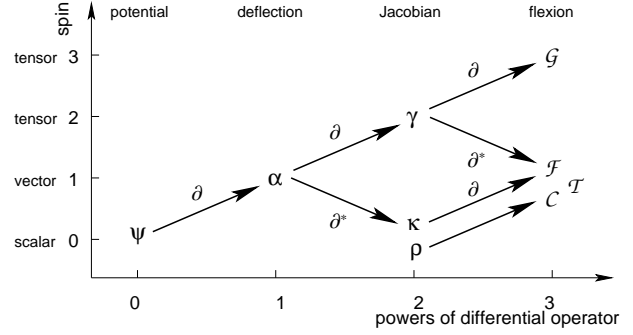


Figure 1. Chart summarising the derivation of the lensing quantities by successive application of the differential operators, and their respective transformation properties.

The surface brightness mapping can now be approximated as

$$\begin{aligned}f_I(\theta_i) &= f_S \left(\delta_{ij} \theta_j + (A_{ij} - \delta_{ij}) \theta_j + \frac{1}{2} D_{ijk} \theta_j \theta_k \right) \\ &\simeq f_S(\theta_i) + (A_{ij} - \delta_{ij}) \theta_j \partial_i f_S(\theta_i) + \frac{1}{2} D_{ijk} \theta_j \theta_k \partial_i f_S(\theta_i).\end{aligned}\quad (24)$$

Figure 1 gives an overview of the lensing quantities, their relationship to the gravitational potential and their transformation properties. C is found by taking the derivative of ρ , but ρ and T do not follow from the potential by taking derivatives. Thus ρ , C and T constitute additional degrees of freedom in the lens mapping beyond gravitational effects.

4 BEHAVIOUR OF TWIST AND TURN

4.1 Rotational Properties

We can now examine how the new constituents of D transform under rotations R , by rotating a source-plane coordinate β_i in the absence of A :

$$\begin{aligned}\beta'_i &= R_{il} D_{lmn} \theta_m \theta_n = R_{il} D_{lmn} R_{mj}^T R_{jp} \theta_p R_{nk}^T R_{kq} \theta_q \\ &= R_{il} D_{lmn} R_{mj}^T R_{nk}^T \theta'_j \theta'_k\end{aligned}\quad (25)$$

where primes denote rotated quantities. But also if D' is the rotated tensor then $\beta'_i = D'_{ijk} \theta'_j \theta'_k$, so

$$D'_{ijk} = R_{il} D_{lmn} R_{mj}^T R_{nk}^T. \quad (26)$$

Since we can write the rotation by angle ϕ as

$$R = \begin{pmatrix} \cos \phi & \sin \phi \\ -\sin \phi & \cos \phi \end{pmatrix} \quad (27)$$

we can write the transformation for D (and its constituent objects) as

$$\begin{aligned}[D'_{ij1}, D'_{ij2}] &= [R_{il} D_{lm1} R_{mj}^T \cos \phi + R_{il} D_{lm2} R_{mj}^T \sin \phi, \\ &\quad -R_{il} D_{lm1} R_{mj}^T \sin \phi + R_{il} D_{lm2} R_{mj}^T \cos \phi]\end{aligned}\quad (28)$$

If we set $F = G = T = C_2 = 0$ so that D only contains non-zero turn C_1 , we find that this C_1 object transforms into the equivalent C_2 object after a $\pi/2$ rotation, and returns to its initial form after a 2π rotation; so C_1 and C_2 are the components of a vector.

Similarly, if we set $F = G = C = T_2 = 0$, the resulting T_1 object transforms into the equivalent T_2 object after a $\pi/2$ rotation, and returns to its initial form after a 2π rotation; so T_1 and T_2 are also the components of a vector.



Figure 2. Effect of 1-flexion and 3-flexion on circular and elliptical ($e = 0.9$) Gaussian sources with $\sigma_{\text{major}} = 0.5''$. Top panel: unlensed objects; middle panel: $F_1 = 0.2 \text{ arcsec}^{-1}$; bottom panel: $G_1 = 0.7 \text{ arcsec}^{-1}$.

4.2 Real Space Behaviour

Now that we have established the rotational properties of the distortions, we would like to visualise what effect they have on real images. We can use the first line of the mapping equation (24) together with the D tensor of equation (23) to observe the effect of the second order image distortions on a Gaussian circular or elliptical image.

Figure 2 shows the effect of 1-flexion and 3-flexion. Here we have operated on objects with Gaussian surface brightness

$$I(\mathbf{x}) = A \exp \left[-\frac{(x - x_c)^2}{2\sigma_x^2} - \frac{(y - y_c)^2}{2\sigma_y^2} \right] \quad (29)$$

where $\sigma_x = \sigma_y = 0.5''$ for the circular source, and $\sigma_x = 0.11''$, $\sigma_y = 0.5''$ for the elliptical source. This gives an ellipticity $e = (\sigma_y^2 - \sigma_x^2)/(\sigma_y^2 + \sigma_x^2) = 0.9$.

Notice that 1-flexion and 3-flexion affect the shape of both circular and elliptical objects in the figure. We can compare this to figure 3, which shows the effect of turn on circular and elliptical objects. Notice that turn has no discernible effect on the circularly symmetric source; we will show later that it indeed has zero effect on such a source. On elliptical objects, turn gives an arc which by eye appears similar to the impact of flexion, but it is truly a different mode of curvature with a distinct estimator which we will find below.

Figure 4 shows the effect of twist. Again, twist appears not to affect circular objects, and we will show this to be the case below. Its impact is to turn elliptical objects into aerofoil shapes. Note the way in which T components engage with ellipticities to make aerofoils oriented in different directions. Positive T_1 or negative T_2 operate to twist horizontal objects into upward curving objects, with the front of the aerofoil pointing in opposite senses; negative T_1 or positive T_2 operate on horizontal objects to make downward curv-



Figure 3. Effect of turn. Top panel: $C_1 = 1.3 \text{ arcsec}^{-1}$ on a circular Gaussian with $\sigma = 0.5''$. Second panel: $C_1 = 1.3 \text{ arcsec}^{-1}$ on elliptical Gaussians with $\sigma_{\text{major}} = 0.5''$, $e_1 = 0.9$ and $e_1 = -0.9$. Third panel: $C_1 = -1.3 \text{ arcsec}^{-1}$ on the same elliptical Gaussians. Fourth panel: $C_2 = 1.3 \text{ arcsec}^{-1}$; Bottom panel: $C_2 = -1.3 \text{ arcsec}^{-1}$.

ing objects. On the other hand, positive T_1 and positive T_2 bend vertical objects to the left, while negative T_1 and negative T_2 bend them to the right.

4.3 Shapelet Space Behaviour

We can gain insight into the behaviour of these distortion modes by examining their action in shapelet space. We use the polar shapelets of Bernstein & Jarvis (2002), Refregier (2003), and Massey & Refregier (2005). As is described in the latter paper, polar shapelets can be described by their number of radial nodes n and



Figure 4. Effect of twist. Top panel: $T_1 = 1.3 \text{ arcsec}^{-1}$ on a circular Gaussian with $\sigma = 0.5''$. Second panel: $T_1 = 1.3 \text{ arcsec}^{-1}$ on elliptical Gaussians $\sigma_{\text{major}} = 0.5''$, $e_1 = 0.9$ and $e_1 = -0.9$. Third panel: $T_1 = -1.3 \text{ arcsec}^{-1}$ on the same elliptical Gaussians. Fourth panel: $T_2 = 1.3 \text{ arcsec}^{-1}$; Bottom panel: $T_2 = -1.3 \text{ arcsec}^{-1}$.

azimuthal nodes m , providing a basis set $|n, m\rangle$ for 2D localised objects. The shapelets require a length scale β to be set, which is the standard deviation of the zeroth shapelet, a 2-D circular Gaussian. Then an image $|f\rangle$ is the sum of the shapelets with appropriate coefficients:

$$|f\rangle = \sum f_{nm} |n, m\rangle \quad (30)$$

and a lensed image is the result of applying various operators to the source:

$$|f'\rangle = (1 + \kappa \hat{K} + \rho \hat{R} + \gamma_i \hat{S}_i + F_i \hat{F}_i + G_i \hat{G}_i + T_i \hat{T}_i + C_i \hat{C}_i) |f\rangle \quad (31)$$

where the terms are for convergence, rotation, shear, 1-flexion, 3-flexion, twist and turn respectively. We wish to discover what these operators are in terms of the ladder operators which act on the basis:

$$\begin{aligned} \hat{a}_r^\dagger |n, m\rangle &= \sqrt{\frac{n+m+2}{2}} |n+1, m+1\rangle \\ \hat{a}_r |n, m\rangle &= \sqrt{\frac{n+m}{2}} |n-1, m-1\rangle \\ \hat{a}_l^\dagger |n, m\rangle &= \sqrt{\frac{n-m+2}{2}} |n+1, m-1\rangle \\ \hat{a}_l |n, m\rangle &= \sqrt{\frac{n-m}{2}} |n-1, m+1\rangle. \end{aligned} \quad (32)$$

The ladder operators obey commutation relations

$$\begin{aligned} [\hat{a}_r, \hat{a}_r^\dagger] &= 1 \\ [\hat{a}_l, \hat{a}_l^\dagger] &= 1 \end{aligned}$$

$$[\hat{a}_l, \hat{a}_r] = [\hat{a}_l, \hat{a}_r^\dagger] = [\hat{a}_l^\dagger, \hat{a}_r] = [\hat{a}_l^\dagger, \hat{a}_r^\dagger] = 0. \quad (33)$$

We can write position and derivative operators in terms of these ladder operators:

$$\begin{aligned} \hat{x} &= \frac{1}{2} [\hat{a}_r^\dagger + \hat{a}_l^\dagger + \hat{a}_l + \hat{a}_r] \\ \hat{y} &= \frac{i}{2} [\hat{a}_r^\dagger - \hat{a}_l^\dagger + \hat{a}_l - \hat{a}_r] \\ \frac{\partial}{\partial x} &= \frac{1}{2} [-\hat{a}_r^\dagger - \hat{a}_l^\dagger + \hat{a}_l + \hat{a}_r] \\ \frac{\partial}{\partial y} &= \frac{i}{2} [-\hat{a}_r^\dagger + \hat{a}_l^\dagger + \hat{a}_l - \hat{a}_r]. \end{aligned} \quad (34)$$

Using these with equation (24), we can find forms for first and second order lensing operators. Massey & Refregier (2005) and Massey et al. (2007) have shown the forms for shear and flexion; these are summarised in figure 5, which shows their effects on a circular Gaussian in shapelet space. Note that shear moves power from the $|0, 0\rangle$ mode to the spin-2 modes $|2, \pm 2\rangle$, while 1-flexion moves power to spin-1 modes, and 3-flexion moves power to the spin-3 modes $|3, \pm 3\rangle$.

We can carry out similar calculations for twist and turn. For twist, after routine but extensive non-commutative algebra we find

$$\begin{aligned} \hat{T}_1 &= -\frac{\beta}{8} \left[(1 - \hat{a}_l^\dagger \hat{a}_l + \hat{a}_r^\dagger \hat{a}_r) \hat{a}_r (1 - i) \right. \\ &\quad - (1 - \hat{a}_r^\dagger \hat{a}_r + \hat{a}_l^\dagger \hat{a}_l) \hat{a}_l (1 + i) \\ &\quad - \hat{a}_r^\dagger (\hat{a}_l^\dagger \hat{a}_l - \hat{a}_r^\dagger \hat{a}_r) (1 + i) \\ &\quad \left. - \hat{a}_l^\dagger (\hat{a}_l^\dagger \hat{a}_l - \hat{a}_r^\dagger \hat{a}_r) (1 - i) \right] \\ \hat{T}_2 &= -\frac{\beta}{8} \left[(1 - \hat{a}_l^\dagger \hat{a}_l + \hat{a}_r^\dagger \hat{a}_r) \hat{a}_r (1 + i) \right. \\ &\quad + (1 - \hat{a}_r^\dagger \hat{a}_r + \hat{a}_l^\dagger \hat{a}_l) \hat{a}_l (1 - i) \\ &\quad + \hat{a}_r^\dagger (\hat{a}_l^\dagger \hat{a}_l - \hat{a}_r^\dagger \hat{a}_r) (1 - i) \\ &\quad \left. - \hat{a}_l^\dagger (\hat{a}_l^\dagger \hat{a}_l - \hat{a}_r^\dagger \hat{a}_r) (1 + i) \right] \end{aligned} \quad (35)$$

where the factor of β takes into account the fact that the operators in equation (34) work in units of β . One can consider what happens to a circular ($m = 0$) source operated on by e.g. \hat{T}_1 ; the third and

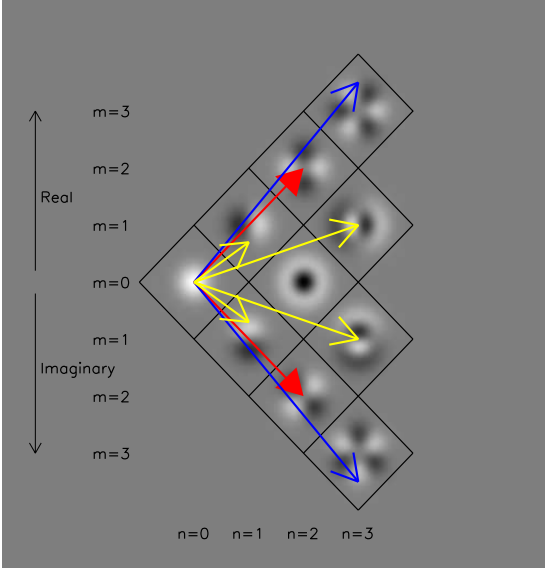


Figure 5. Effect of shear and flexion on a circular Gaussian in shapelet space. Shapelet profiles are displayed for the real part of polar shapelets in the top part of the figure, and for the imaginary part in the bottom part of the figure. Shear (red) takes power from the Gaussian shapelet $|0, 0\rangle$ and places it in the spin-2 modes $|2, \pm 2\rangle$. 1-Flexion (yellow) moves power to spin-1 modes, while 3-Flexion (blue) moves power to the spin-3 modes $|3, \pm 3\rangle$.

fourth terms in the equation above for \hat{T}_1 vanish, as $(\hat{a}_l^\dagger \hat{a}_l - \hat{a}_r^\dagger \hat{a}_r)$ counts m ; the first term initially acts with a_r to move the state to a spin-1 state; then the term in brackets $(1 - \hat{a}_l^\dagger \hat{a}_l + \hat{a}_r^\dagger \hat{a}_r)$ operates to give zero. The second term similarly gives zero, resulting in twist having no effect on circularly symmetric objects.

The effect of these operators is shown in figure 6. Since they have no impact for circular objects, we show the effect on the $|2, 2\rangle$ mode. Note that power is moved to neighbouring spin 1 and spin 3 modes, with a rotation of $(1 + i)$ or $(1 - i)$ which gives the characteristic twisted form of the image.

We carry out similar calculations for turn, again using operators given by equation (34) together with the mapping equation (24). We find

$$\begin{aligned} \hat{C}_1 &= \frac{i\beta}{8} \left[- \left(1 + \hat{a}_l^\dagger \hat{a}_l - \hat{a}_r^\dagger \hat{a}_r \right) \hat{a}_l + \left(1 + \hat{a}_r^\dagger \hat{a}_r - \hat{a}_l^\dagger \hat{a}_l \right) \hat{a}_r \right. \\ &\quad \left. - \hat{a}_l^\dagger \left(\hat{a}_l^\dagger \hat{a}_l - \hat{a}_r^\dagger \hat{a}_r \right) + \hat{a}_r^\dagger \left(\hat{a}_r^\dagger \hat{a}_r - \hat{a}_l^\dagger \hat{a}_l \right) \right] \\ \hat{C}_2 &= -\frac{\beta}{8} \left[- \left(1 + \hat{a}_l^\dagger \hat{a}_l - \hat{a}_r^\dagger \hat{a}_r \right) \hat{a}_l - \left(1 + \hat{a}_r^\dagger \hat{a}_r - \hat{a}_l^\dagger \hat{a}_l \right) \hat{a}_r \right. \\ &\quad \left. + \hat{a}_l^\dagger \left(\hat{a}_l^\dagger \hat{a}_l - \hat{a}_r^\dagger \hat{a}_r \right) + \hat{a}_r^\dagger \left(\hat{a}_r^\dagger \hat{a}_r - \hat{a}_l^\dagger \hat{a}_l \right) \right] \quad (36) \end{aligned}$$

Here again we find that the impact on $m = 0$ states is zero, using an identical argument to above. The effect of these operators is shown in figure 7. Again we show the effect on the $|2, 2\rangle$ mode; as for twist, power is moved to neighbouring spin 1 and spin 3 modes, but there are a different range of activated modes for C_1 and C_2 , due to the different factors of i .

Now that we can describe twist and turn in shapelet space, we are in a position to construct practical estimators for measuring these quantities.

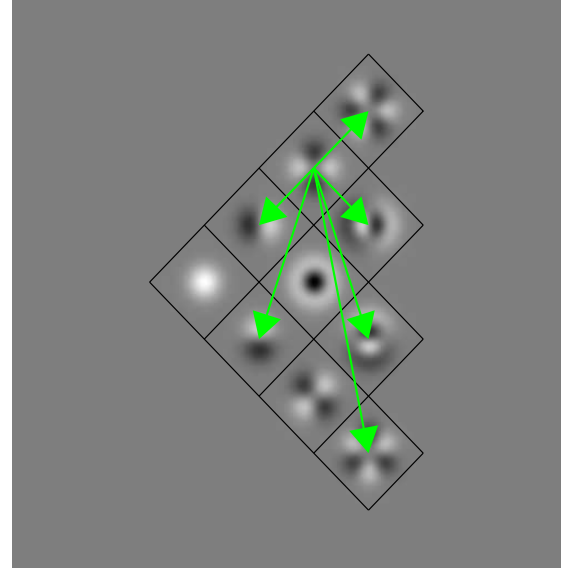


Figure 6. Effect of twist in shapelet space. Circular Gaussians are not affected, so here we show the power moved from the $|2, 2\rangle$ mode; note that twist pushes power into spin 1 and spin 3 modes.

5 MEASURING TWIST AND TURN

5.1 Simple Estimators

We can use the ladder operator form for twist to find a simple estimator. Considering the power that finishes in the f_{11} component,

$$f'_{11} = f_{11} - \frac{\beta}{2} e^{-i\pi/4} T_1 f_{22} \quad (37)$$

where f'_{11} is the component after twist. Since the mean untwisted f_{11} is expected to be zero, we have the estimator

$$T_1^{\text{est}} = -\frac{2}{\beta} e^{i\pi/4} \frac{f_{11}}{f_{22}} \quad (38)$$

Similarly, we find

$$T_2^{\text{est}} = -\frac{2}{\beta} e^{-i\pi/4} \frac{f_{11}}{f_{22}} \quad (39)$$

In a similar fashion, the turned f_{11} coefficient is given by

$$f'_{11} = f_{11} + \frac{i\beta}{2\sqrt{2}} C_1 f_{22} \quad (40)$$

so since the undistorted mean f_{11} is expected to be zero, we obtain the estimator

$$C_1^{\text{est}} = -\frac{2\sqrt{2}i}{\beta} \frac{f_{11}}{f_{22}} \quad (41)$$

and similarly

$$C_2^{\text{est}} = \frac{2\sqrt{2}}{\beta} \frac{f_{11}}{f_{22}} \quad (42)$$

This concludes our initial proposal for estimators.

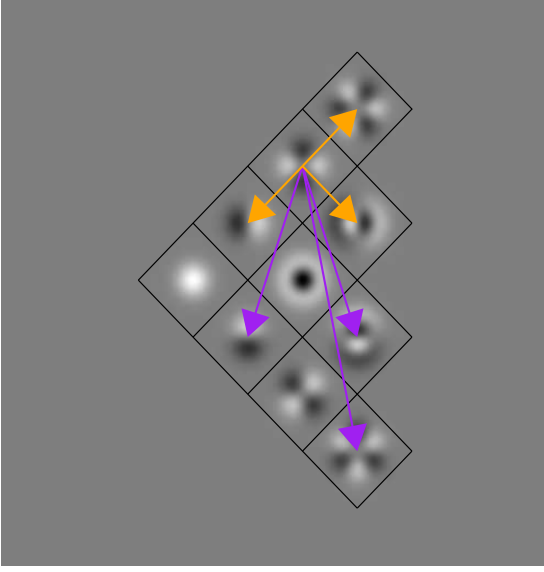


Figure 7. Effect of turn in shapelet space. As for twist, circular Gaussians are not affected, so we again show the power moved from the $|2, 2\rangle$ mode. The C_1 component (purple) pushes power into spin 1 and spin 3 modes on the opposite side of the diagram, while C_2 (orange) does the same on the near side of the diagram.

5.2 Correction for Centroid Shift

Unfortunately these simple estimators need correcting for the fact that twist and turn move the centroid of the object. Goldberg & Bacon (2005) show that the centroid is moved by the D tensor according to

$$\begin{aligned}\Delta\bar{\theta}_1 &= -\langle\theta_1^2\rangle\left(\frac{3}{2}D_{111} + \frac{1}{2}D_{212} + \frac{1}{2}D_{221}\right) \\ &\quad -\langle\theta_1\theta_2\rangle(D_{112} + D_{121} + D_{222}) - \langle\theta_2^2\rangle\frac{1}{2}D_{122} \\ \Delta\bar{\theta}_2 &= -\langle\theta_1^2\rangle\frac{1}{2}D_{211} - \langle\theta_1\theta_2\rangle(D_{221} + D_{212} + D_{111}) \\ &\quad -\langle\theta_2^2\rangle\left(\frac{3}{2}D_{222} + \frac{1}{2}D_{121} + \frac{1}{2}D_{112}\right)\end{aligned}\quad (43)$$

where we have written a form which assumes less symmetry than Goldberg & Bacon; this is necessary for our generalised D tensor. Putting the values of the D tensor, equation (23), into this equation we find

$$\Delta\bar{\theta}_1 + i\Delta\bar{\theta}_2 = \frac{R^2}{4\beta} [6F + 5F^*e^* + Ge^* + iC^*e + (i-1)Te] \quad (44)$$

where R^2 is the size quadrupole and e is the unweighted ellipticity as given in Massey et al. (2007). Note again that for circular ($e = 0$) objects, twist and turn have no effect.

Massey et al. (2007) showed that the effect of the centroid shift is to alter observable flexion estimators $\hat{F}_1 + i\hat{F}_2$ by subtracting a term $(\Delta\bar{\theta}\hat{D}_r + \Delta\bar{\theta}^*\hat{D}_l)$, and the same applies here. The shift operators \hat{D} are given by

$$\hat{D}_r = \frac{1}{2}(a_r^\dagger - a_l) \quad \hat{D}_l = \frac{1}{2}(a_l^\dagger - a_r) \quad (45)$$

Hence we find that equation (37) becomes

$$\begin{aligned}f'_{11} &= f_{11} - \frac{\beta}{2}e^{-i\pi/4}T_1f_{22} \\ &\quad + \frac{R^2}{8\beta}T_1[(i-1)(e_1 + ie_2)(f_{00} - f_{20}) \\ &\quad + \sqrt{2}(i+1)(e_1 - ie_2)f_{22}]\end{aligned}\quad (46)$$

By dividing both sides by f_{22} , we can therefore propose the corrected estimator

$$T_1^{\text{est}} = -\frac{2}{\beta}e^{i\pi/4}\frac{f_{11}}{f_{22}}\left(1 + \left\langle\frac{R^2(e_1 + ie_2)(f_{00} - f_{20})}{2\sqrt{2}\beta^2f_{22}}\right\rangle\right)^{-1} \quad (47)$$

If we label the term in brackets as B , we similarly find

$$T_2^{\text{est}} = -\frac{2}{B\beta}e^{-i\pi/4}\frac{f_{11}}{f_{22}} \quad (48)$$

For the turns we find

$$C_1^{\text{est}} = -\frac{2\sqrt{2}i}{B\beta}\frac{f_{11}}{f_{22}} \quad C_2^{\text{est}} = \frac{2\sqrt{2}}{B\beta}\frac{f_{11}}{f_{22}} \quad (49)$$

So our corrected estimators differ from our naive estimators only by a factor of B .

6 FIRST MEASUREMENTS OF TWIST AND TURN

We are now in a position to measure twist and turn on real data. We use the STAGES mosaic observed with the Hubble Space Telescope (Gray et al. 2007; Heymans et al. 2008). This is a 0.25 square degree field observed with the Advanced Camera for Surveys in the F606W band, covering 80 ACS tiles in 80 orbits. Drizzling is used to obtain an effective pixel size of $0.03''$.

We use the same galaxy catalogue as Heymans et al. (2008), deconvolving and decomposing all objects into shapelets using the methods developed in Refregier (2003); Refregier & Bacon (2003); Massey & Refregier (2005). The analysis will be described in full in Bacon et al (2008); we obtain a shapelet catalogue for 56,000 galaxies, together with measures of β and R^2 for all objects. The shapelets are normalised so that $f_{00} = 1$.

We estimate the twist and turn for all objects using equations (47) to (49); we find that for our survey, $B = 2.47 \pm 0.01$. The resulting histograms of twist and turn measurements are shown in figures 8 and 9; these include 3σ cuts for outliers with $|T| > 11.3 \text{ arcsec}^{-1}$ and $|C| > 16.2 \text{ arcsec}^{-1}$, and we only consider objects with $\beta > 1$ pixel to avoid oversampling. The first thing to note is that twist and turn are more noisy than shear and flexion; twist components have a standard deviation of 3.8 arcsec^{-1} , while turn components have a standard deviation of 5.4 arcsec^{-1} .

We find mean values over the STAGES survey of $\bar{T}_1 = 0.002 \pm 0.016 \text{ arcsec}^{-1}$, $\bar{T}_2 = 0.004 \pm 0.016 \text{ arcsec}^{-1}$, $\bar{C}_1 = -0.003 \pm 0.023 \text{ arcsec}^{-1}$, and $\bar{C}_2 = -0.011 \pm 0.022 \text{ arcsec}^{-1}$. All of these are consistent with zero, as we might hope for a systematic mode. At present the constraint is fairly weak, as gravitational flexion signals are at the level of 0.001 to 0.01 arcsec^{-1} ; however, in upcoming lensing surveys the much larger area will lead to twist and turn constraints at the 10^{-5} level, which will provide important checks on systematics.

We can further explore whether twist and turn are activated as systematics in the STAGES survey by measuring their correlation functions. As with shear correlation functions, the twists and turns should be rotated before they are correlated; however, while shear has to be rotated by factors of $e^{i2\phi}$ where ϕ is the position angle of

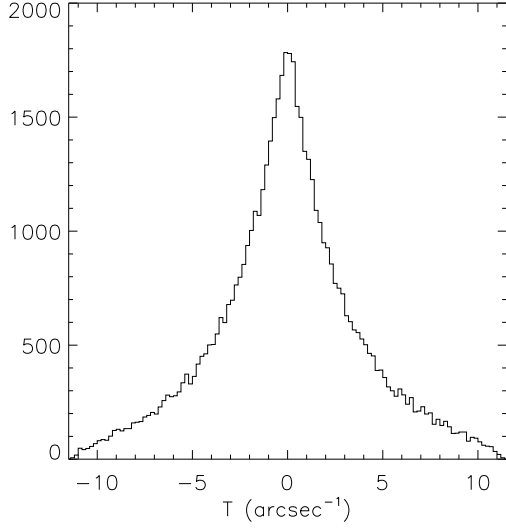


Figure 8. Histogram of twist values in the STAGES survey, for objects with $|T| < 11.3 \text{ arcsec}^{-1}$ and $\beta > 1$ pixel.

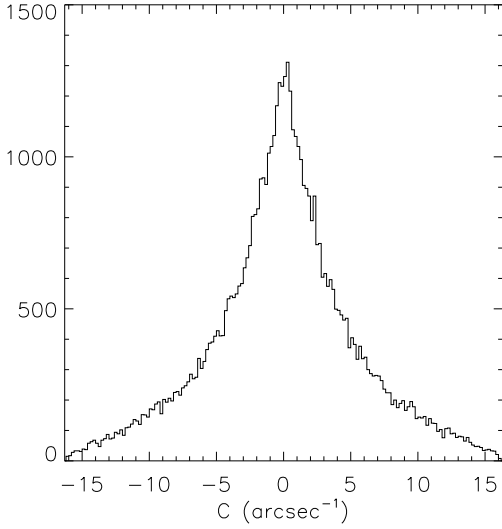


Figure 9. Histogram of turn values in the STAGES survey, for objects with $|C| < 16.2 \text{ arcsec}^{-1}$ and $\beta > 1$ pixel.

the line joining a pair of objects, twist and turn have to be rotated by factors of $e^{i\phi}$ on account of their vector nature:

$$\begin{aligned} T_1^{\text{rot}} &= T_1 \cos \phi + T_2 \sin \phi \\ T_2^{\text{rot}} &= -T_1 \sin \phi + T_2 \cos \phi \end{aligned} \quad (50)$$

We can then construct correlation functions

$$\begin{aligned} C_{11}^T(\theta) &= \langle T_1^{\text{rot}}(\vec{\theta}_i) T_1^{\text{rot}}(\vec{\theta}_i + \vec{\theta}) \rangle \\ C_{22}^T(\theta) &= \langle T_2^{\text{rot}}(\vec{\theta}_i) T_2^{\text{rot}}(\vec{\theta}_i + \vec{\theta}) \rangle \\ C_{12}^T(\theta) &= \langle T_1^{\text{rot}}(\vec{\theta}_i) T_2^{\text{rot}}(\vec{\theta}_i + \vec{\theta}) \rangle \end{aligned} \quad (51)$$

and in an analogous fashion we can construct turn correlation functions C_{ij}^C . We have measured these correlation functions for twist and turn in STAGES, and display the results in fig-

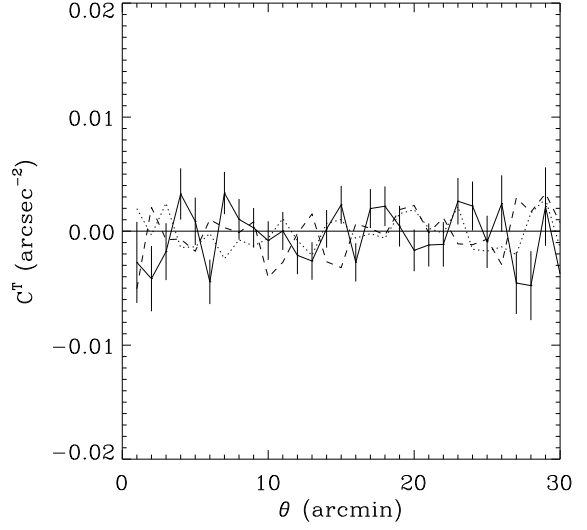


Figure 10. STAGES twist correlation function. Solid line: $\langle T_1 T_1 \rangle$ correlation function. Dashed line: $\langle T_2 T_2 \rangle$ correlation function. Dotted line: $\langle T_1 T_2 \rangle$ correlation function.

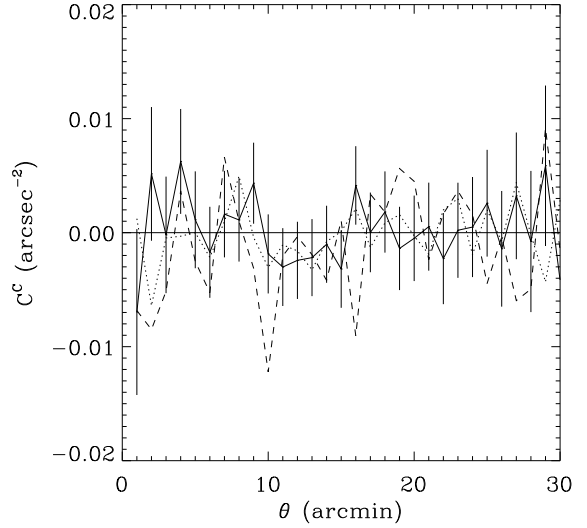


Figure 11. STAGES turn correlation function. Solid line: $\langle C_1 C_1 \rangle$ correlation function. Dashed line: $\langle C_2 C_2 \rangle$ correlation function. Dotted line: $\langle C_1 C_2 \rangle$ correlation function.

ures 10 and 11. Here error bars are estimated by $\sigma^2 / \sqrt{N_{\text{pairs}}}$ where σ is the standard deviation of twist or turn and N_{pairs} is the number of galaxy pairs in a bin. We find that the correlation functions are almost all consistent with zero signal, with $\chi^2 = 38.3, 27.3, 13.9, 12.5, 43.1, 8.8$ for 30 bins in θ for $C_{11}^T, C_{22}^T, C_{12}^T, C_{11}^C, C_{22}^C$, and C_{12}^C respectively. The largest positive outlier here is for C_{22}^C ; the signal is primarily due to the 3.5σ value at 10 arcmin; we should treat this as a warning of the possible existence of systematics at this scale for flexion.

7 CONCLUSION

In this paper, we have written down for the first time the full weak image distortion relevant to weak lensing, to second order. This involved the discovery of two new image distortions, the twist and the turn.

We reviewed weak lensing distortions to first order, recouching the lens mapping in terms of Pauli matrices. We noted the existence of a non-gravitational mode, the rotation. This sets a precedent which we also see at second order.

We then extended the formalism to second order; at this point it became clear that the gradient of the rotation gives a new mode, which we call the turn. A further mode was found by seeking a combination of Pauli matrices orthogonal to all known modes; this new mode was called the twist. We were then able to write down the full image distortion mapping to second order.

We explored the properties of twist and turn, finding that both are vector quantities. Their visual effect was shown, as was their impact in shapelet space. With the ladder operator formalism we showed that neither twist nor turn has any effect on circularly symmetric objects, but only objects with non-zero ellipticity. We saw how twist and turn move power from spin-2 modes to modes with spin-1 and spin-3.

Using our ladder operator forms for twist and turn, we found simple estimators for the two distortions; however, twist and turn cause a centroid shift which needs to be taken into account. This leads to the inclusion of a common factor B in the estimators for twist and turn.

We used these estimators to measure twist and turn for the first time in the HST STAGES survey. We noted that these distortions have a larger intrinsic noise scatter compared to 1- or 3-flexion, but their mean values across the survey are already at an interesting level for checking large flexion systematics. We found that mean twist and turn are consistent with zero in this survey. We measured twist and turn correlation functions, and found that they too were consistent with zero in almost all cases.

The two quantities introduced in this study complete the set of distortions to second order. They will be of use in testing for systematic effects, and have a certain elegance of their own.

8 ACKNOWLEDGEMENTS

We would like to thank Kathy Bacon, Meghan Gray, Alan Heavens, Catherine Heymans and Barnaby Rowe for useful discussions, and the STAGES collaboration for use of their data. DB is funded by an STFC Advanced Fellowship and an RCUK Research Fellowship.

REFERENCES

- Arfken G. B., Weber H. J., 2005, *Mathematical methods for physicists* 6th ed.. Materials and Manufacturing Processes
- Bacon D. J., Goldberg D. M., Rowe B. T. P., Taylor A. N., 2006, *MNRAS*, 365, 414
- Bartelmann M., Schneider P., 2001, *Phys. Rep.*, 340, 291
- Bernstein G. M., Jarvis M., 2002, *AJ*, 123, 583
- Goldberg D. M., Bacon D. J., 2005, *ApJ*, 619, 741
- Goldberg D. M., Natarajan P., 2002, *ApJ*, 564, 65
- Gray M., Aragon-Salamanca A., Bacon D., Balogh M., Barazza F. D., Barden M., Bell E., Beswick R., et al. 2007, in *American Astronomical Society Meeting Abstracts Vol. 211 of American Astronomical Society Meeting Abstracts, STAGES: Space Telescope A901/902 Galaxy Evolution Survey*. p. 132.20
- Heymans C., Gray M. E., Peng C. Y., van Waerbeke L., Bell E. F., Wolf C., Bacon D., Balogh M., et al. 2008, *MNRAS*, 385, 1431
- Irwin J., Shmakova M., 2005, *New Astronomy Review*, 49, 83
- Massey R., Refregier A., 2005, *MNRAS*, 363, 197
- Massey R., Rowe B., Refregier A., Bacon D. J., Bergé J., 2007, *MNRAS*, 380, 229
- Okura Y., Umetsu K., Futamase T., 2008, *ApJ*, 680, 1
- Refregier A., 2003, *MNRAS*, 338, 35
- Refregier A., Bacon D., 2003, *MNRAS*, 338, 48
- Schneider P., Er X., 2008, *A&A*, 485, 363
- Arfken G. B., Weber H. J., 2005, *Mathematical methods for physicists* 6th ed.. Materials and Manufacturing Processes
- Bacon D. J., Goldberg D. M., Rowe B. T. P., Taylor A. N., 2006, *MNRAS*, 365, 414
- Bartelmann M., Schneider P., 2001, *Phys. Rep.*, 340, 291
- Bernstein G. M., Jarvis M., 2002, *AJ*, 123, 583
- Goldberg D. M., Bacon D. J., 2005, *ApJ*, 619, 741
- Goldberg D. M., Natarajan P., 2002, *ApJ*, 564, 65
- Gray M., Aragon-Salamanca A., Bacon D., Balogh M., Barazza F. D., Barden M., Bell E., Beswick R., et al. 2007, in *American Astronomical Society Meeting Abstracts Vol. 211 of American Astronomical Society Meeting Abstracts, STAGES: Space Telescope A901/902 Galaxy Evolution Survey*. p. 132.20
- Heymans C., Gray M. E., Peng C. Y., van Waerbeke L., Bell E. F., Wolf C., Bacon D., Balogh M., et al. 2008, *MNRAS*, 385, 1431
- Irwin J., Shmakova M., 2005, *New Astronomy Review*, 49, 83
- Massey R., Refregier A., 2005, *MNRAS*, 363, 197
- Massey R., Rowe B., Refregier A., Bacon D. J., Bergé J., 2007, *MNRAS*, 380, 229
- Okura Y., Umetsu K., Futamase T., 2008, *ApJ*, 680, 1
- Refregier A., 2003, *MNRAS*, 338, 35
- Refregier A., Bacon D., 2003, *MNRAS*, 338, 48
- Schneider P., Er X., 2008, *A&A*, 485, 363